



# Extreme temperature influence on low velocity impact damage and residual flexural properties of CFRP

Irene Bavasso<sup>1</sup>  | Claudia Sergi<sup>1</sup>  | Luca Ferrante<sup>2</sup> | Marzena Pawlik<sup>3</sup> | Yiling Lu<sup>3</sup> | Luca Lampani<sup>4</sup> | Jacopo Tirillò<sup>1</sup> | Fabrizio Sarasini<sup>1</sup>

<sup>1</sup>Department of Chemical Engineering Materials Environment, Sapienza-Università di Roma & UdR INSTM, Rome, Italy

<sup>2</sup>ENEA Italian National Agency for New Technologies, Energy and Sustainable Economic Development, Italy

<sup>3</sup>College of Science and Engineering, University of Derby, Derby, UK

<sup>4</sup>Department of Mechanical and Aerospace Engineering, Sapienza-Università di Roma, Rome, Italy

## Correspondence

Irene Bavasso, Department of Chemical Engineering Materials Environment, Sapienza-Università di Roma & UdR INSTM, Via Eudossiana 18, Roma 00184, Italy.  
Email: [irene.bavasso@uniroma1.it](mailto:irene.bavasso@uniroma1.it)

## Abstract

In this work, the behavior of carbon fiber reinforced polymer composites (CFRPs) interleaved with electrospun veils under low velocity impact (LVI) conditions and extreme environmental temperatures was investigated. 2/2 twill carbon fiber/epoxy laminates were subjected to LVI at three energy levels (10, 20, and 30 J), and three temperatures ( $-50^{\circ}\text{C}$ , room temperature, and  $100^{\circ}\text{C}$ ). Two interleaved configurations were explored (six veils placed symmetrically with respect to the middle plane of the laminate and with respect to the external layers of the laminate). Particularly at room temperature and up to 20 J, nanofibrous interlayers effectively reduced localized deformation (by about 13.0%) and delamination (by about 12.2%) when positioned in the outer ply interleaved configuration compared to the reference laminate. At  $100^{\circ}\text{C}$ , this effect is maintained at 10 J, preventing an increase in the delaminated area. At  $-50^{\circ}\text{C}$  and 10 J, the promotion of delamination prevented back surface fiber failure. Regarding post-impact flexural properties, the presence of nanoveils ensured superior mechanical properties compared to the corresponding reference laminate impacted at the same conditions, demonstrating their efficacy in enhancing the damage tolerance of the overall laminate.

## Highlights

- Electrospun veils were interleaved in 20 layers of 2/2 twill carbon/epoxy laminate.
- Three configurations were tested under LVI at 10 J, 20 J, 30 J, and  $-50^{\circ}\text{C}$ , RT, and  $100^{\circ}\text{C}$ .
- Observed damage modes include delamination, indentation, and back surface fiber cracks.
- Veils symmetrically placed in external layers limit delamination at 20 J (RT) and 10 J ( $100^{\circ}\text{C}$ ).
- Electrospun veils enhanced CFRP bending and residual post-impact properties at RT and  $100^{\circ}\text{C}$ .

## KEYWORDS

carbon fibers, damage tolerance, electrospun veils, interleaving, low velocity impact tests, residual properties

This is an open access article under the terms of the [Creative Commons Attribution](https://creativecommons.org/licenses/by/4.0/) License, which permits use, distribution and reproduction in any medium, provided the original work is properly cited.

© 2024 The Author(s). *Polymer Composites* published by Wiley Periodicals LLC on behalf of Society of Plastics Engineers.

## 1 | INTRODUCTION

Carbon fiber reinforced polymer composites (CFRP) represent a class of materials attractive for several applications<sup>1</sup> thanks to their outstanding mechanical properties, including stiffness and strength, all within a product of low density.<sup>2</sup> The research community dedicated to optimize CFRP structures and their manufacturing, is addressing a primary challenge associated with these materials, that is, delamination resistance, because of their layered structure and limited out-of-plane performance<sup>3,4</sup> especially under low velocity impact (LVI) conditions when barely visible damages (BVD) are induced.<sup>5–7</sup> One of the strategies currently under investigation involves incorporating thermoplastic polymer nanofibers as toughening agents in the interlaminar region to enhance the composite's toughness without adding weight or increasing laminate thickness.<sup>8</sup> Since 2001, there has been a growing interest in the use of nanoveils produced through electrospinning thanks to Dzenis and Reneker who patented the production of polybenzimidazole electrospun fibers as reinforcing veils placed between graphite/epoxy prepreg laminae.<sup>9</sup> Their work showcased the effectiveness of this approach, employing a versatile and controllable method. In the context of insoluble interleaves, polyamide is an example.<sup>10</sup> Several studies in the literature explored the assessment of CFRP interleaved with such type of electrospun veils under various test conditions, for example, tensile,<sup>11</sup> three-point bending,<sup>12,13</sup> Mode I interlaminar fracture toughness,<sup>14–26</sup> Mode II interlaminar fracture toughness,<sup>10,17,19,20,27</sup> short-beam shear.<sup>12</sup>

As regards LVI conditions, there is limited literature available on this subject, with only a few papers addressing the evaluation of damage tolerance in CFRP at various impact energy levels considering the positioning of electrospun veils. Akangah et al. conducted research evaluating the incorporation of electrospun Nylon-66 nanofabric between two consecutive layers of carbon fiber prepreg and epoxy resin arranged in a quasi-isotropic sequence [0/45/90/–45]<sub>2S</sub>. Their study demonstrated the effectiveness of such veils in reducing damage growth (as matrix cracks and delamination) up to an impact energy level of 1.8 J.<sup>15</sup> Moreover, Palazzetti et al.<sup>28</sup> and Sarasini et al.<sup>29</sup> investigated the advantages of strategically placing electrospun nanofibers only in areas where the highest delamination occurs in neat CFRP. In the first study,<sup>28</sup> the introduction of three veils at the lowest interface or four veils placed symmetrically to the middle plane of the laminate, that is, ten layers of carbon fiber prepreg and epoxy resin in a unidirectional stacking sequence, resulted in a reduction of the delaminated area extent up to an impact energy level of 12 J. This highlighted the self-stiffening and self-repair effect provided by the nanofibrous

interlayers. In the second study,<sup>29</sup> a different stacking sequence was tested, that is, unidirectional carbon/epoxy prepreg stacked in a cross-ply configuration [0/90]<sub>4S</sub>. Interleaving four electrospun veils symmetrically with respect to the middle plane of the laminate allowed the extent of delaminated area to be reduced. This was attributed to the veils acting as bridges between consecutive layers thus exerting a positive toughening effect and contributing to additional energy dissipation mechanisms.

All the mentioned investigations were conducted only at room temperature. It is widely recognized that temperature, in conjunction with the impact energy level, can significantly influence the damage propagation mechanisms due to the difference in thermal expansion coefficients between carbon fiber and resin, leading to the generation of thermal stresses.<sup>10</sup> For example, in aircraft applications, the external surface of an aircraft is subjected to varying temperatures during take-off and landing, reaching low temperatures of approximately –58°C<sup>30</sup> and high temperatures of around 70°C.<sup>10</sup> Therefore, assessing the performance of carbon/epoxy laminates under such extreme temperatures is essential to offer a more comprehensive understanding of the state-of-the-art in this field.

In CFRP, the effect of low-velocity events at high temperatures has been investigated by Suvarna et al.<sup>31</sup> who conducted tests on a laminate consisting of sixteen layers of carbon fiber epoxy with [0/90/90/0]<sub>2S</sub> layup at a velocity of 2 m/s, corresponding to an impact energy of 4.3 J, up to 90°C. This study revealed a decrease in delaminated area extent as the temperature increased and a higher post-impact residual strength. This phenomenon was attributed to the blunting crack effect of the matrix, which appears to be more deformable approaching its glass transition temperature. Additionally, Körbelin et al.,<sup>3</sup> in laminates with a [45/0/–45/90]<sub>2S</sub> configuration tested at impact energy levels ranging from 8 to 21 J and temperatures between 20 and 80°C, highlighted a more significant occurrence of fiber breakage at the impacted side at elevated temperatures, attributed to the high compressive load.

The low-temperature environments promote delamination and significant damage such as perforation,<sup>32</sup> as observed by Papa et al.<sup>33</sup> under impact conditions of 10 J and –25°C in a laminate with seven layers of carbon fabric with a [0/90] stacking sequence. The CFRP performance under such conditions is strongly influenced by the embrittlement of the epoxy resin and interlaminar thermal stresses, which are intensified by laminate architectures like cross-ply and quasi-isotropic layouts up to –150°C.<sup>34</sup>

Concerning CFRP interleaved with electrospun polyamide nanofibers, no studies on their impact behavior as a function of the operating temperature are available. Only Saeedifar et al.<sup>27</sup> conducted Mode II interlaminar fracture toughness tests on 24 layers of unidirectional carbon/epoxy

prepregs. The study demonstrated that the presence of the nano-layer contributed to promoting  $G_{IIC}$  compared to the virgin laminate. This enhancement remained consistent up to 100°C, which was close to the adopted curing temperature. Beyond this temperature, a decrease in  $G_{IIC}$  for the nano-modified specimens was observed. This reduction was attributed to the severe plastic deformation of nanofibers, although the modified specimens continued to exhibit higher values than those of the virgin laminate.

The objective of this work is to provide a comprehensive analysis of the response of CFRP interleaved with electrospun veils under LVI conditions and extreme operating temperatures. For the first time, 20 layers of 2/2 twill carbon fiber/epoxy prepreg laminate were tested considering two different interleaved configurations, three different impact energy levels (10, 20, and 30 J) and three temperatures (−50°C, room temperature and 100°C). The results of the interleaved configurations were examined in terms of force-displacement curves, energy absorption along with the assessment of damage evolution (delaminated area, dent depth), and compared with the performances of the virgin laminate. Four-point bending tests were also conducted to evaluate the post-impact residual flexural properties of the laminates and fracture surface analysis through scanning electron microscopy (SEM) was carried out to detail the effect of electrospun veils.

## 2 | EXPERIMENTAL

### 2.1 | Materials and composite manufacturing

A 2/2 twill carbon/epoxy prepreg (XPREG<sup>®</sup>XC130, 210 g/m<sup>2</sup>, Easy Composites, UK) was used for the fabrication of the composite laminates. The composites were interleaved using commercially available electrospun veils provided by Revolution Fibers (Xantu.Layr<sup>®</sup>) with an areal density of 4.5 g/m<sup>2</sup>.<sup>29</sup> After laminating 20 layers of carbon fiber prepreg, the specimens were manufactured

by vacuum bagging and autoclave forming (1 h at 120°C and 7 bar). The glass transition temperature of the epoxy resin after the curing cycle is expected to be around 120°C according to the technical datasheet. Three configurations were considered (Figure 1): the virgin laminate (named C) and two interleaved laminates where six veils were used and placed symmetrically with respect to the middle plane of the laminate (named CN6C) and symmetrically with respect to the external layers of the laminate (named CN6E).

### 2.2 | Composites characterization

Low-velocity impact tests (ISO 6603-2) were performed using a CEAST/Instron 9340 drop-weight impact testing machine equipped with a hemispherical tip (12.7 mm diameter). The kinetic impact energy was adjusted by varying the release height of the weight (3.055 kg) and specimens were clamped between two steel plates with a circular unsupported area (40 mm as diameter). All tests were performed in triplicate at three energy levels (10, 20, and 30 J) and three temperature conditions (−50°C, room temperature and 100°C). The specimens (150 × 100 mm) were pre-conditioned for 1 h in the thermostatic chamber at test temperature.

The through-the-thickness damaged area was determined as a sum of the damaged area in each layer by ultrasonic tests through Omni Scan MX2 equipment with a sound speed of 3020 m/s (3.5 MHz as phased array probe, 64 elements, pitch 1 mm, active aperture 64 mm, elevation 7 mm, water immersion with 25 mm water wedge). Non-contact laser profilometer (Talyscan 150, Taylor Hobson) was used to measure the dent depth after impact tests at a scanning speed of 8500 μm/s.

Bending properties were evaluated through four-point bending tests according to ASTM D 6272 on specimens measuring 150 × 40 × 4 mm, using a Zwick/Roell Z010 universal testing machine. The width was adapted to include the damage induced by low velocity impacts. Tests

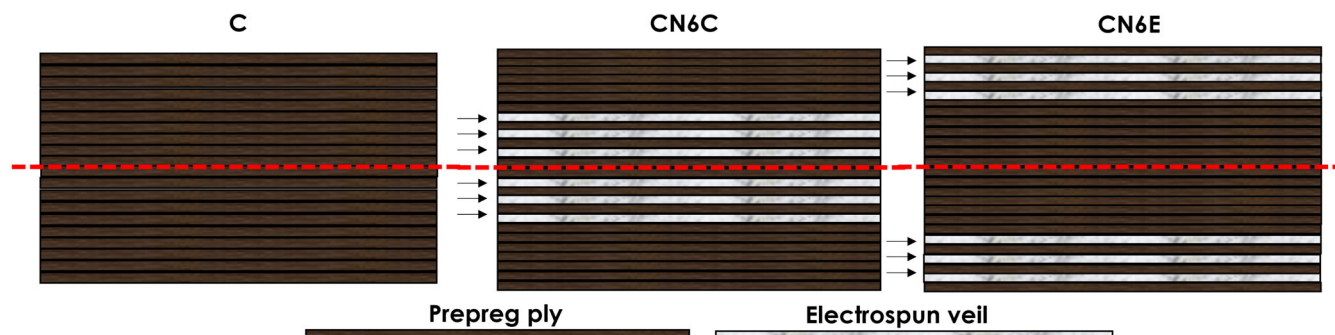
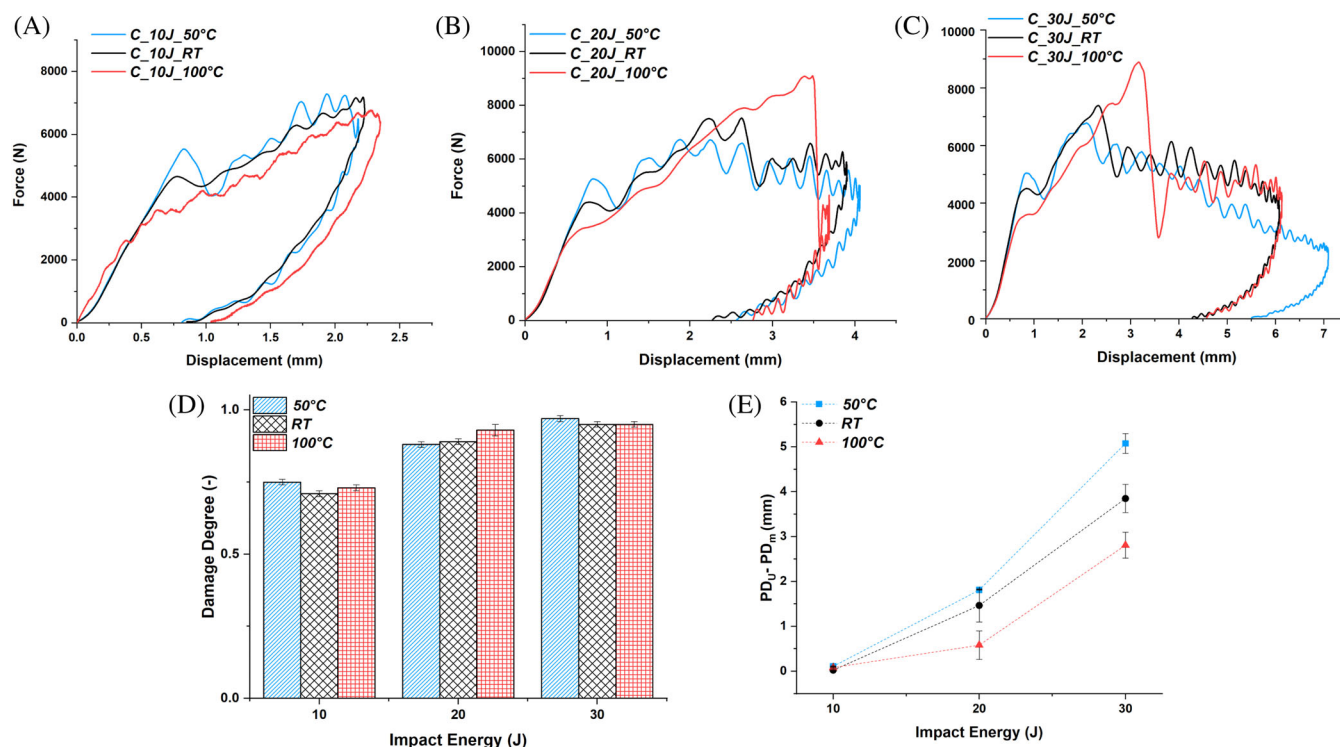


FIGURE 1 Schematic view of the tested configurations (the electrospun veils were placed at the position marked by the arrow).



**FIGURE 2** Effect of temperature during LVI test on C laminate: Force versus displacement trends at (A) 10 J, (B) 20 J and (C) 30 J, (D) Damage Degree and (E) structural integrity index.

were conducted in displacement control (2.5 mm/min cross-head speed) on both non-impacted and impacted specimens, with the impacted side facing the compression load. The support span was 120 mm while the distance between the loading noses was set at 60 mm.

Composite fracture morphology was detailed via SEM using a Tescan MIRA3. Prior to examination, all specimens underwent sputter coating with gold.

### 3 | RESULTS AND DISCUSSION

#### 3.1 | LVI results and post-impact properties of non-interleaved laminates

In Figure 2, the outcomes of impact tests conducted on control CFRP specimens as a function of impact energy and operating temperatures are reported. The results are illustrated through force-versus-displacement curves in Figure 2A–C while Figure 2D shows the calculated damage degree (ratio of the absorbed energy to the impact energy). Furthermore, in Figure 2E, the structural integrity index,<sup>35</sup> evaluated as difference between PDU (ultimate displacement) and PDM (displacement at the peak force), is showcased.

The closed curves in Figure 2A–C indicate that perforation did not occur up to an impact energy of 30 J at all

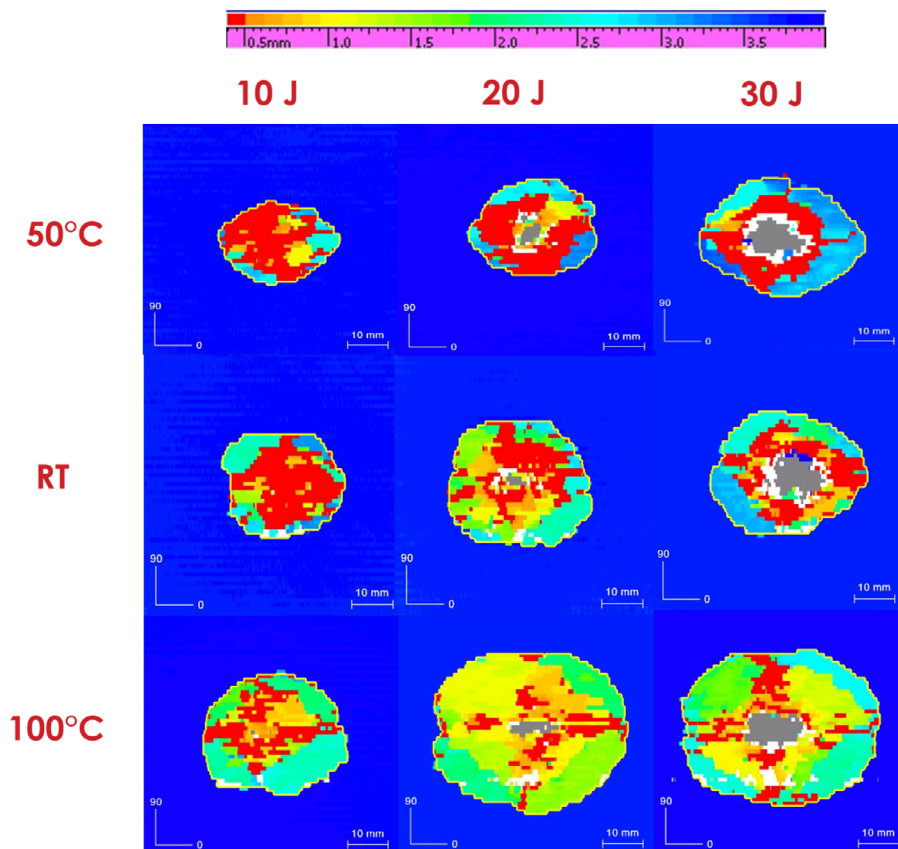
tested temperatures, as evidenced by the rebound of the impactor. Moreover, the impact curves clearly highlight that the laminates exhibited a distinct response for different combinations of impact energy and operating temperature. Despite the subtle differences in damage degree (Figure 2D), the load drops observed during the loading phase in the force versus displacement trends imply potential differences in the produced damage and the energy dissipation mechanisms involved.

As a preliminary confirmation of this observation, the structural integrity index (Figure 2E) was examined and the results reveal that at the lowest temperature, the material experiences a significant loss of integrity. To understand the behavior of C laminates during impact events at various temperatures, it is important to note that: (i) it is expected a transition from a more brittle response of the laminate at low temperatures ( $-50^{\circ}\text{C}$ )<sup>34,36–38</sup> to a more compliant one at high temperatures ( $100^{\circ}\text{C}$ ) due to the progressive approach of matrix glass transition temperature<sup>3,39,40</sup>; (ii) in addition, when subjected to low temperatures, the fiber–matrix interface becomes much weaker<sup>41</sup> and this contributes to increased stress concentration and residual stresses, resulting in a decrease in quasi-static mechanical performance.<sup>42</sup>

In particular, the first consideration helps explain the findings obtained from the impact at 10 J (Figure 2A, Table 1), as evidenced by the increase in peak force and

**TABLE 1** Summary of LVI data and post-impact delaminated area and dent depth values at the different temperature and energy conditions.

Sample	Onset of damage (kN)	Peak force (kN)	Maximum displacement (mm)	Delaminated area (mm <sup>2</sup> )	Dent depth (μm)
Impact energy 10 J					
<i>C</i> <sub>-50°C</sub>	5.85 ± 0.24	7.37 ± 0.66	2.15 ± 0.08	486.39 ± 6.84	112.10 ± 4.24
<i>C</i> <sub>RT</sub>	4.84 ± 0.21	7.24 ± 0.11	2.18 ± 0.03	603.83 ± 92.25	184.53 ± 3.70
<i>C</i> <sub>100°C</sub>	3.58 ± 0.08	6.74 ± 0.52	2.36 ± 0.02	761.27 ± 98.70	235.85 ± 24.25
Impact energy 20 J					
<i>C</i> <sub>-50°C</sub>	5.97 ± 0.32	7.77 ± 0.43	3.93 ± 0.01	652.41 ± 88.04	765.76 ± 18.00
<i>C</i> <sub>RT</sub>	5.14 ± 0.10	8.16 ± 0.31	3.80 ± 0.12	721.80 ± 92.63	771.63 ± 16.03
<i>C</i> <sub>100°C</sub>	3.63 ± 0.10	8.88 ± 0.48	3.74 ± 0.19	1100.20 ± 38.37	610.83 ± 65.60
Impact energy 30 J					
<i>C</i> <sub>-50°C</sub>	5.89 ± 0.36	7.37 ± 0.32	7.20 ± 0.46	963.43 ± 34.31	-
<i>C</i> <sub>RT</sub>	5.10 ± 0.08	7.85 ± 0.37	6.03 ± 0.14	826.88 ± 80.91	1815.67 ± 38.50
<i>C</i> <sub>100°C</sub>	4.14 ± 0.12	9.08 ± 0.36	5.85 ± 0.19	1504.04 ± 86.28	1351.51 ± 67.09

**FIGURE 3** C-scans of C laminates impacted at different energy and temperature levels.

the decrease in maximum displacement with decreasing temperature. Even if the results from LVI tests did not show significant differences in terms of absorbed energy, there was a noticeable variation in the type and extent of damage. Upon preliminary visual inspection (Figure S1), an initial extent of fiber fracture was observed at the

back side of the laminate impacted at the lowest temperature ( $-50^{\circ}\text{C}$ ; white arrow in Figure S1). This observation is further supported by more pronounced load drops (after reaching the onset of damage force value reported in Table 1) during the loading phase in the curves in Figure 2A.<sup>43</sup>

This occurs because, at  $-50^{\circ}\text{C}$ , the stiffer matrix contributes to higher stress concentrations in the impacted area thus making the material less prone to deformation and leading to through-the-thickness damage. This hypothesis is further confirmed by the C-scan analysis shown in Figure 3. Although the delaminated area is relatively smaller compared to the results obtained at room temperature and  $100^{\circ}\text{C}$ , it is notable that delamination predominantly affects the layers near the impact point (as indicated by the red-colored area). Moreover, the appearance of the back crack on  $-50^{\circ}\text{C}$  impacted samples highlights an onset of damage caused mainly by the approach of laminates elastic limit in bending which is responsible for fibers failure in tension. Additionally, interlaminar thermal stresses arise due to the constrained ply transverse contraction.<sup>34</sup>

These effects are less pronounced at room temperature: the improvement in CFRP properties and better interfacial fiber-matrix adhesion<sup>41,42</sup> help to reduce stress concentration, preventing fiber failure in tension on the back face. On the other hand, at  $100^{\circ}\text{C}$ , such fluctuations are smoothed out, and the damage becomes visible in compression, characterized by a superior indentation as indicated in Table 1. These findings align with results collected from experiments conducted on glass fiber/epoxy laminates subjected to comparable operating conditions,<sup>36,37</sup> as well as on carbon fiber/epoxy laminates with cross-ply stacking sequences exposed to temperatures as low as  $-25^{\circ}\text{C}$  with impact energies of  $7.5\text{ J}$ <sup>46</sup> and  $10\text{ J}$ .<sup>33</sup> In these experiments, it was observed that the reduction in operating temperature had a significant impact on the extent of damage.

C-scan results in Figure 3, along with the data of delaminated area extent provided in Table 1, reveal a superior delaminated area during the impact at  $100^{\circ}\text{C}$  and its gradual reduction with decreasing impact temperature. Again, even if the extent of delaminated area for  $100^{\circ}\text{C}$  impacted samples is higher than room temperature and  $-50^{\circ}\text{C}$  ones, it is necessary to highlight that the delamination at the highest temperature concentrates mostly in the upper half of the specimen, thus disclosing a higher damping capability of the material which allows to prevent the through the thickness damage. In particular, the progressive decrease in laminate stiffness makes it more compliant towards the deformation imposed by the impactor and allows to increase the volume of the specimen which reacts to the impact.

In summary, the impact damage in all cases consists of a combination of shear and transverse ply cracks leading to delamination and back surface fiber cracking.<sup>31,42</sup> However, while back surface fiber cracking is the primary consuming energy damage mechanism at low temperature ( $-50^{\circ}\text{C}$ ), delamination becomes predominant at higher temperatures due to the progressive approach of

matrix glass transition temperature which makes the laminate more compliant towards bending deformation. In addition, the different thermal expansion characteristics (CTE) of carbon fibers and epoxy resin<sup>39,45</sup> contribute to the occurrence of interlaminar shear stresses. The softening of the matrix at  $100^{\circ}\text{C}$  proves ineffective in transferring loads to adjacent plies, thus diminishing the reinforcing effect of the fibers<sup>46</sup> and consequently reducing the peak force measured during impacts at  $10\text{ J}$ . As the impact energy increases, lower temperatures significantly compromise the integrity of the laminates (Figure 2E) while, despite the larger delaminated area observed at  $100^{\circ}\text{C}$ , the extensive matrix deformation helps blunting cracks throughout the thickness,<sup>31</sup> thereby preserving higher peak force values.

On the contrary, the observed trend in terms of delamination extension with temperature in this study differs from what has been noted in previous papers.<sup>31,33,34</sup> However, this discrepancy can be attributed to the fact that in those works LVI test involves impact energy levels below  $10\text{ J}$  or temperatures up to  $-20^{\circ}\text{C}$ , conditions where delamination may prevail as the dominant damage mode compared to back surface cracking. As the impact energy level increases, there is a notable reduction in the damage tolerance of the laminate, accompanied by an increase in the loss of structural integrity (Figure 2E) at all investigated temperatures. The measured peak force shows a progressive increase at higher impact energy levels, especially at  $20\text{ J}$ . However, at room temperature and  $-50^{\circ}\text{C}$ , a slight decrease in peak force compared to  $20\text{ J}$  is recorded, attributed to the reduction in laminate resistance to impacts at

**TABLE 2** Summary of flexural properties of C laminates before and after the impact.

Sample	Flexural strength (MPa)	Flexural modulus (GPa)
Non impacted		
C	$710.63 \pm 23.53$	$55.49 \pm 0.87$
Impact energy 10 J		
C <sub>-50°C</sub>	$367.69 \pm 31.33$	$49.63 \pm 2.12$
C <sub>RT</sub>	$436.42 \pm 21.99$	$53.36 \pm 0.26$
C <sub>100°C</sub>	$419.05 \pm 29.11$	$54.07 \pm 1.63$
Impact energy 20 J		
C <sub>-50°C</sub>	$350.86 \pm 16.25$	$48.52 \pm 1.29$
C <sub>RT</sub>	$385.73 \pm 20.01$	$50.01 \pm 0.59$
C <sub>100°C</sub>	$309.64 \pm 7.28$	$49.79 \pm 1.79$
Impact energy 30 J		
C <sub>-50°C</sub>	$320.36 \pm 15.28$	$43.80 \pm 1.85$
C <sub>RT</sub>	$255.84 \pm 21.43$	$40.07 \pm 2.96$
C <sub>100°C</sub>	$263.26 \pm 26.00$	$41.31 \pm 3.96$

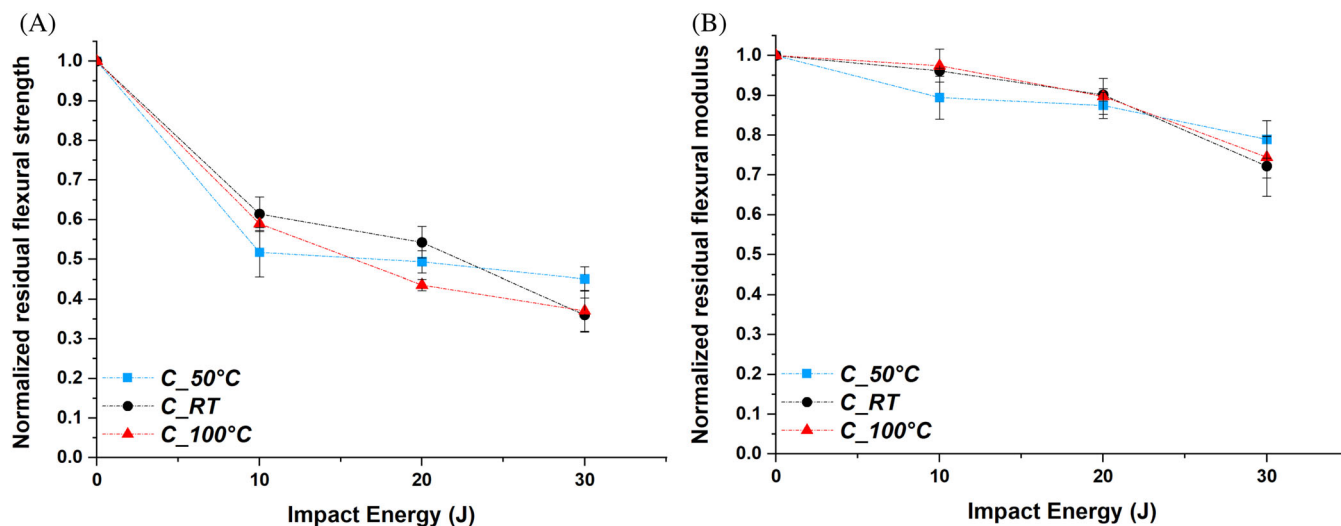


FIGURE 4 Normalized residual flexural strength (A) and (B) modulus after the impact of C laminates as a function of impact energy and temperature.

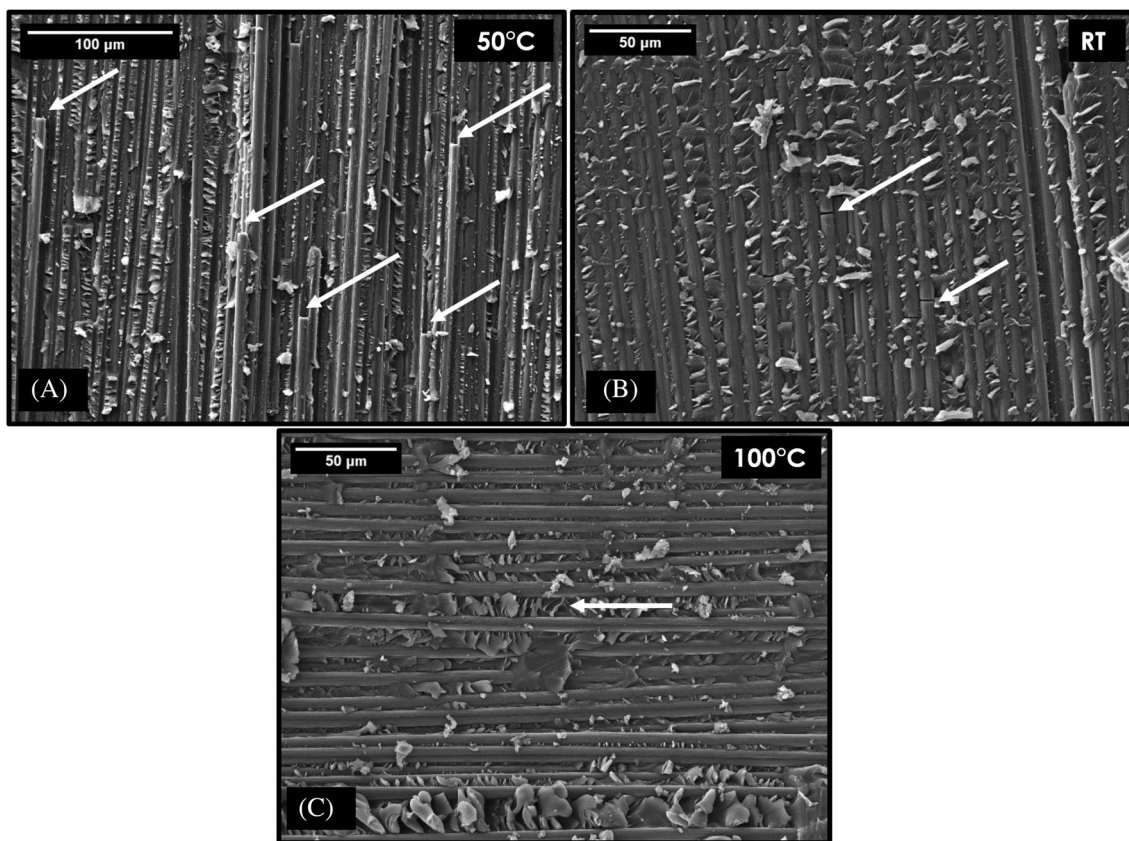
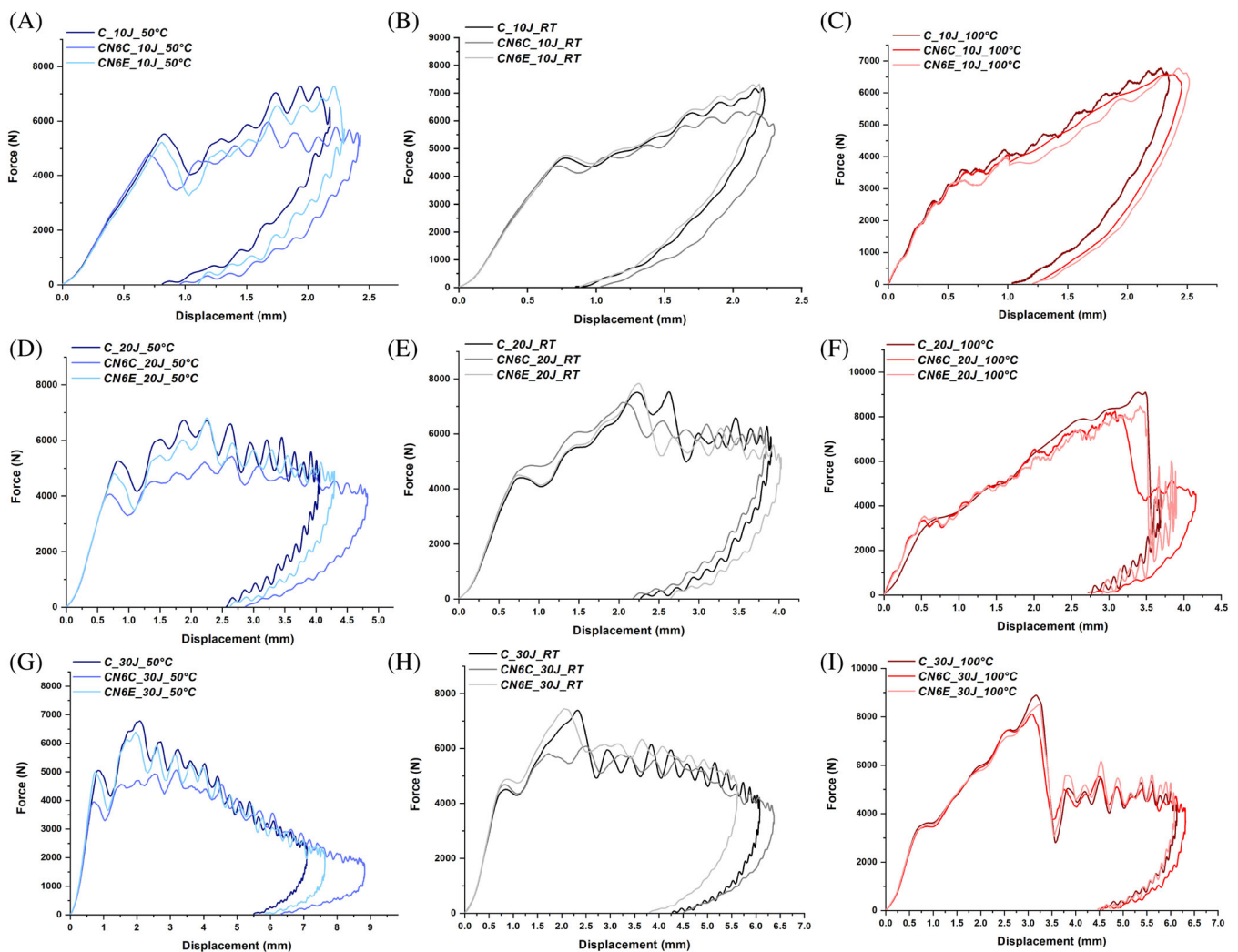


FIGURE 5 Fracture surfaces after flexural tests of C laminates impacted at different temperatures.

30 J. This is further supported by high localized deformation, as indicated by the significant dent depth values measured in these specimens (Table 1), with a notable extent of matrix and fiber breakage as observed in Figure S2. Indeed, the increased permanent indentation is strictly correlated to fibers breakage as significant penetration

phenomena start to intervene thus determining a significant loss in laminate structural integrity.

What is noteworthy is the correlation between the increase in impact energy levels (and impact velocity from 2.55 to 4.43 m/s) and the extent of the delaminated area at all investigated temperatures, with the involvement of the



**FIGURE 6** Effect of temperature on force vs. displacement trends during LVI tests on interleaved laminates at (A, B, C) 10 J, (D, E, F) 20 J and (G, H, I) 30 J.

bottom layer of the laminate particularly evident at the lowest temperature (Figure 3). At 100°C, it can be inferred that delamination affects only progressively the layers through-the-thickness for increasing impact energies, starting from the upper surface due to the previously discussed “delayed” impact. On the contrary, at room temperature and –50°C, the gradual increase in matrix brittleness leads to a decrease in the extent of delaminated area but distributes it through the whole thickness of the laminate as confirmed by the delamination on both compression (indicated by the red-colored area) and tension (indicated by the blue-colored area) sides. This phenomenon is driven by both stiffness mismatching and the displacement of broken and unbroken fibers. These observations are similar to the findings reported by Sergi et al.,<sup>44</sup> where comparable trends were noted in both the extent of delaminated area and the value of indentation depth already from impact energy levels in the range 2.5 J–7.5 J. This is probably due to the small

specimens' thickness (2 mm) compared to that of laminates examined in the current study. Liu et al.<sup>39</sup> have observed that at lower temperatures (as –25°C), the embrittlement of the epoxy matrix leads to increased damage to both the matrix and the carbon fibers that appears circular in shape when viewed from the top or bottom, because of the hemispherical shape of the impactor. However, when temperatures rise (around 50°C), the resin softens, resulting in less breakage of the carbon weave and reduced overall damage to the material. Analogous results were found by Icten et al. in glass/epoxy laminates subjected to low-velocity impact (LVI) conditions and temperatures ranging from 20 to –60°C.<sup>47</sup>

Regarding the post-impact properties of the specimens, four-point bending tests were conducted on C laminates after the impact, and the results, including flexural strength and modulus, were compared with those of non-impacted laminates. The results are summarized in



**TABLE 3** Summary of LVI data and post-impact delaminated area and dent depth values at the different temperatures and energy conditions for interleaved laminates.

Sample	Onset of damage (kN)	Peak force (kN)	Maximum displacement (mm)	Delaminated area (mm <sup>2</sup> )	Dent depth (μm)
Impact energy 10 J					
CN6C <sub>-50°C</sub>	5.18 ± 0.46	6.32 ± 0.47	2.41 ± 0.10	1335.46 ± 51.07	161.25 ± 1.48
CN6C <sub>RT</sub>	4.61 ± 0.05	6.72 ± 0.21	2.22 ± 0.04	1042.41 ± 23.92	167.86 ± 10.72
CN6C <sub>100°C</sub>	3.55 ± 0.11	6.56 ± 0.08	2.38 ± 0.02	1075.30 ± 154.30	253.85 ± 5.44
CN6E <sub>-50°C</sub>	5.56 ± 0.05	7.64 ± 0.41	2.22 ± 0.01	590.86 ± 61.98	146.05 ± 14.07
CN6E <sub>RT</sub>	5.07 ± 0.05	7.47 ± 0.05	2.12 ± 0.02	508.49 ± 29.08	166.30 ± 2.55
CN6E <sub>100°C</sub>	3.75 ± 0.28	6.81 ± 0.11	2.39 ± 0.06	758.81 ± 94.25	228.05 ± 0.35
Impact energy 20 J					
CN6C <sub>-50°C</sub>	4.99 ± 0.35	7.37 ± 0.66	4.60 ± 0.12	1765.49 ± 13.98	383.10 ± 11.76
CN6C <sub>RT</sub>	6.35 ± 0.03	7.24 ± 0.11	3.75 ± 0.04	1001.85 ± 72.68	603.57 ± 11.12
CN6C <sub>100°C</sub>	3.34 ± 0.04	6.74 ± 0.52	4.08 ± 0.06	1575.09 ± 17.89	770.67 ± 25.39
CN6E <sub>-50°C</sub>	5.59 ± 0.13	7.64 ± 0.62	4.12 ± 0.04	759.17 ± 12.07	598.03 ± 22.52
CN6E <sub>RT</sub>	5.84 ± 0.91	8.18 ± 0.15	3.76 ± 0.12	633.04 ± 61.83	671.97 ± 7.86
CN6E <sub>100°C</sub>	3.53 ± 0.09	8.54 ± 0.42	3.90 ± 0.03	1482.52 ± 89.46	696.30 ± 32.06
Impact energy 30 J					
CN6C <sub>-50°C</sub>	5.26 ± 0.21	7.37 ± 0.66	9.47 ± 0.90	1887.79 ± 42.81	-
CN6C <sub>RT</sub>	6.35 ± 0.23	7.24 ± 0.11	6.38 ± 0.16	1478.23 ± 18.77	1990.33 ± 26.10
CN6C <sub>100°C</sub>	3.95 ± 0.13	6.74 ± 0.52	6.13 ± 0.09	1511.84 ± 25.78	1792.66 ± 16.35
CN6E <sub>-50°C</sub>	5.91 ± 0.38	7.16 ± 0.34	7.18 ± 0.37	1569.86 ± 9.64	-
CN6E <sub>RT</sub>	7.67 ± 0.30	7.99 ± 0.23	5.51 ± 0.10	897.84 ± 70.17	1983.66 ± 24.39
CN6E <sub>100°C</sub>	3.98 ± 0.16	8.80 ± 0.37	6.06 ± 0.19	1595.96 ± 40.42	1812.33 ± 27.48

Table 2, and normalized values (with respect to the results of the non-impacted sample) are reported in Figure 4. In brief, as anticipated, the occurrence of damages after the impact event led to a reduction in the bending properties of all tested laminates. At 10 J, fiber failure notably contributed to a significant decrease in the damage tolerance of C<sub>-50°C</sub> compared to the other laminates impacted at room temperature and 100°C. With a further increase in the impact energy level, there was a more substantial reduction in bending strength for C<sub>RT</sub> and C<sub>100°C</sub>, while in C<sub>-50°C</sub>, the normalized strength nearly flattened. This difference is attributed to the fact that during bending tests, failure is primarily governed by the crack propagation on the surface in compression from the edge of the sample to the indentation point. In C<sub>RT</sub> and C<sub>100°C</sub>, the upper layers experienced superior damage during LVI tests. Concerning the bending modulus, the trends are quite similar to those of the bending strength. However, the modulus was less affected by the impact event, showing only a slight reduction in normalized residual modulus. This is because localized damage and delamination do not have a direct impact on the initial force/deflection trend.<sup>48</sup>

Fracture surface analysis (Figure 5) of impacted specimens after bending tests showed clean fiber surfaces with minimal matrix residue and characteristic hackle marks typical of fiber-resin adhesive failure (Mode II fracture, indicated by the white arrow in Figure 5C). The occurrence of fiber failure is prominently visible in specimens impacted at the lowest temperature, as indicated by the white arrows in Figure 5A,B.

### 3.2 | LVI results and post-impact properties of interleaved laminates

Six electrospun nano-veils were interleaved in C laminates symmetrically with respect to the outer layers (CN6E) and with respect to the middle plane of the laminate (CN6C). The specimens were tested according to the same experimental campaign conducted for C laminates to ensure a direct comparison of the results. Force vs. displacement curves are presented in Figure 6, where it can be observed that the introduction of the veils did not lead to significant differences in the impact response of the laminates, and their overall

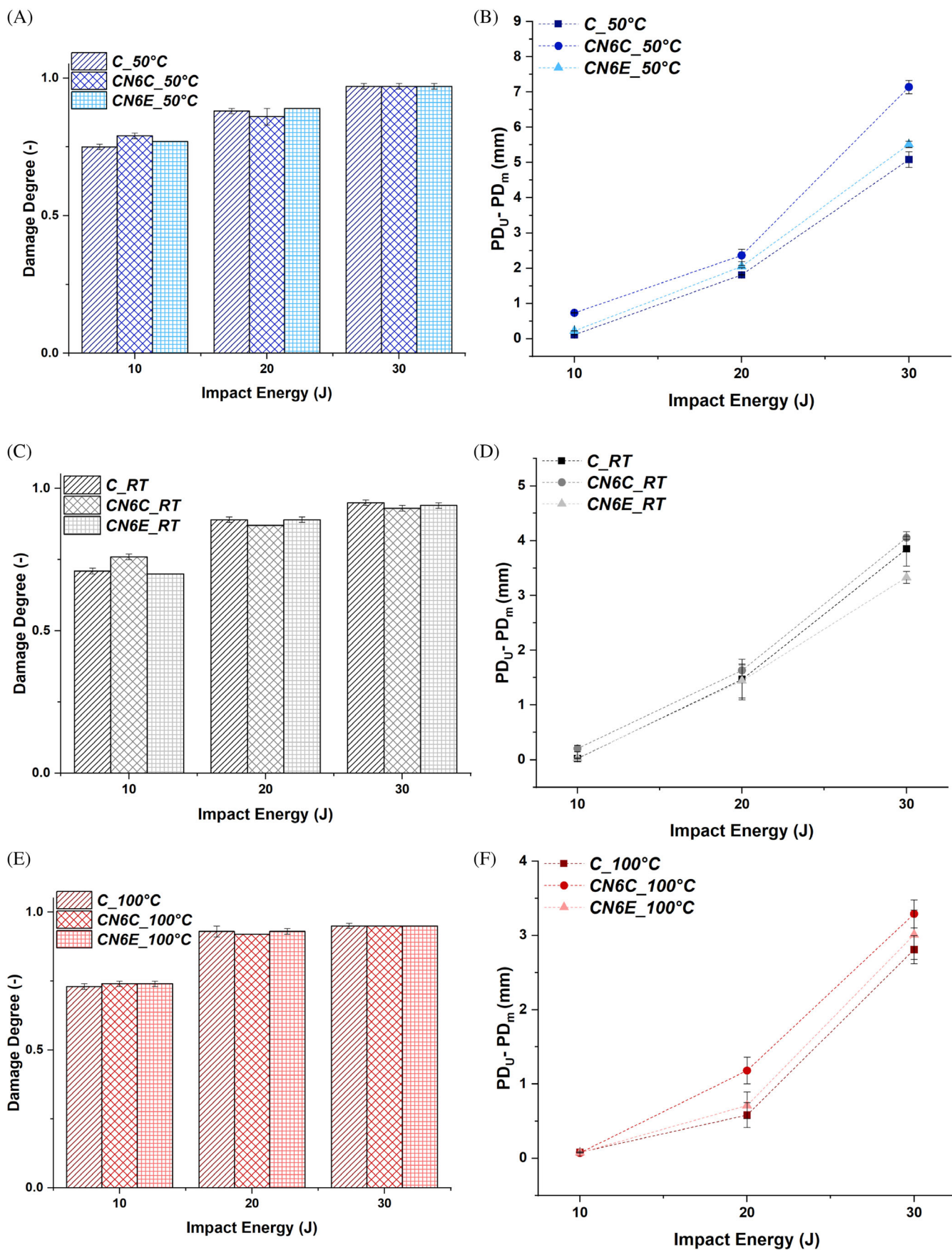


FIGURE 7 Effect of temperature and impact energy on (A, C, E) damage degree and (B, D, F) structural integrity index.

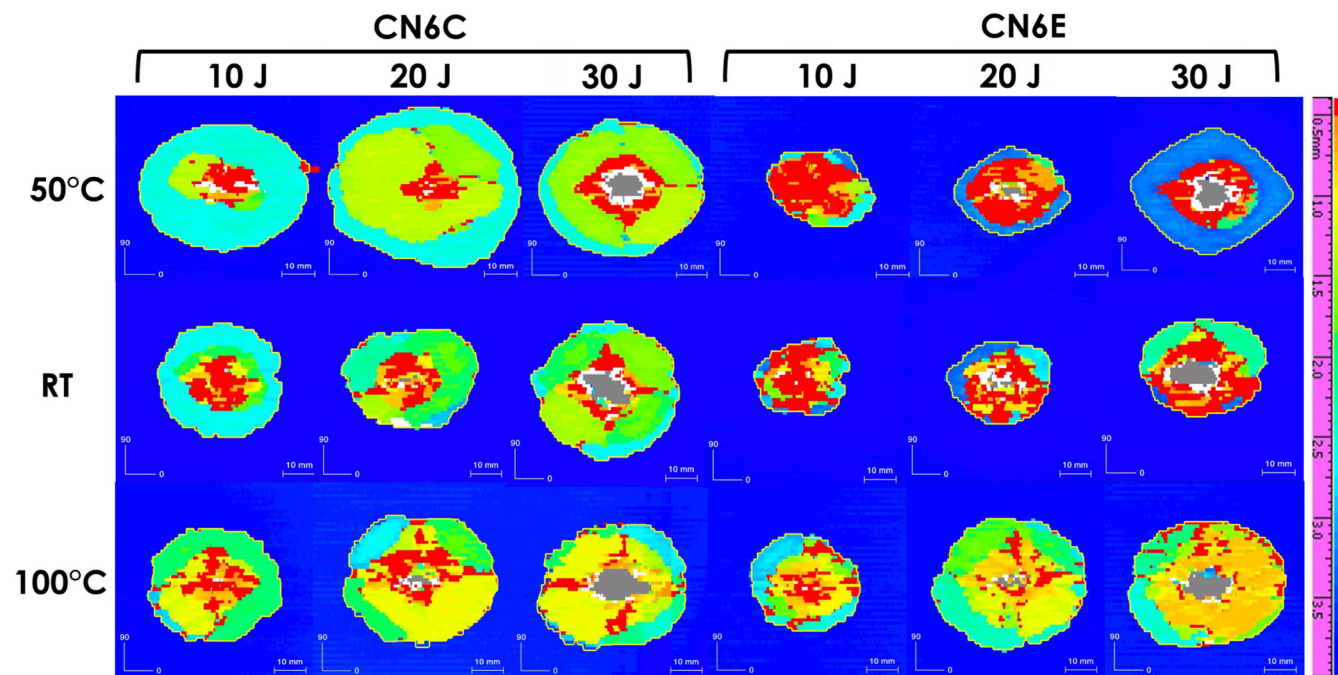


FIGURE 8 C-scans of CN6C and CN6E laminates impacted at different energy and temperature levels.

trends remained similar, especially at room temperature and 100°C.

At room temperature, the CN6E configuration demonstrated greater effectiveness in improving interlaminar fracture toughness, as evidenced by the superior values of the onset damage and peak forces (Table 3) at all impact energy levels. Specifically, the peak force was found to be marginally affected, increasing by approximately 3.66% (−50°C), 3.17% (RT), and 1.04% (100°C) at 10 J, and 1.78% (RT) at 30 J. Additionally, the onset peak force rose by about 4.75% (10 J), 13.61% (20 J), and 50.39% (30 J) at room temperature. The maximum displacement was slightly reduced only at room temperature.

This improvement was not observed for the CN6C configuration where actually a decrease in these parameters was detected compared to the C configuration. In addition, when considering the results in terms of displacement (Table 3), the presence of the veils symmetrically with respect to the middle plane contributed to a slightly superior loss of integrity (Figure 7B,D,F). The interleaved laminates absorbed a comparable amount of energy to the C configuration, resulting in a similar damage degree (Figure 7A,C,E). However, even in this case, the resulting damage was different.

The analysis of damages, including delamination (Table 3, Figure 8), and dent depth (Table 3) points out the contribution of the electrospun veils. At room temperature and up to 20 J, the localized deformation was reduced by approximately 9.8% (10 J) and 13.0% (20 J) for

TABLE 4 Summary of flexural properties of interleaved laminates before and after the impact.

Sample	Flexural strength (MPa)	Flexural modulus (GPa)
Non impacted		
CN6C	708.17 ± 1.89	56.57 ± 2.88
CN6E	778.49 ± 9.53	62.50 ± 1.67
Impact energy 10 J		
CN6C <sub>−50°C</sub>	437.95 ± 24.27	58.26 ± 0.10
CN6C <sub>RT</sub>	473.99 ± 38.25	57.17 ± 0.75
CN6C <sub>100°C</sub>	419.21 ± 15.44	55.10 ± 0.92
CN6E <sub>−50°C</sub>	465.06 ± 11.65	55.55 ± 0.57
CN6E <sub>RT</sub>	549.20 ± 8.54	59.58 ± 1.01
CN6E <sub>100°C</sub>	470.47 ± 78.66	57.93 ± 2.44
Impact energy 20 J		
CN6C <sub>−50°C</sub>	308.54 ± 4.59	49.52 ± 0.57
CN6C <sub>RT</sub>	395.16 ± 20.18	54.97 ± 1.64
CN6C <sub>100°C</sub>	313.64 ± 19.20	48.36 ± 0.83
CN6E <sub>−50°C</sub>	365.53 ± 30.74	49.96 ± 0.41
CN6E <sub>RT</sub>	425.65 ± 11.38	52.19 ± 1.37
CN6E <sub>100°C</sub>	327.99 ± 26.34	51.17 ± 1.65
Impact energy 30 J		
CN6C <sub>−50°C</sub>	185.31 ± 34.34	35.99 ± 3.83
CN6C <sub>RT</sub>	296.41 ± 25.69	45.83 ± 2.29
CN6C <sub>100°C</sub>	267.96 ± 4.83	44.66 ± 2.49
CN6E <sub>−50°C</sub>	271.81 ± 2.30	44.69 ± 1.30
CN6E <sub>RT</sub>	333.82 ± 5.30	48.65 ± 1.13
CN6E <sub>100°C</sub>	267.79 ± 15.80	45.93 ± 0.98

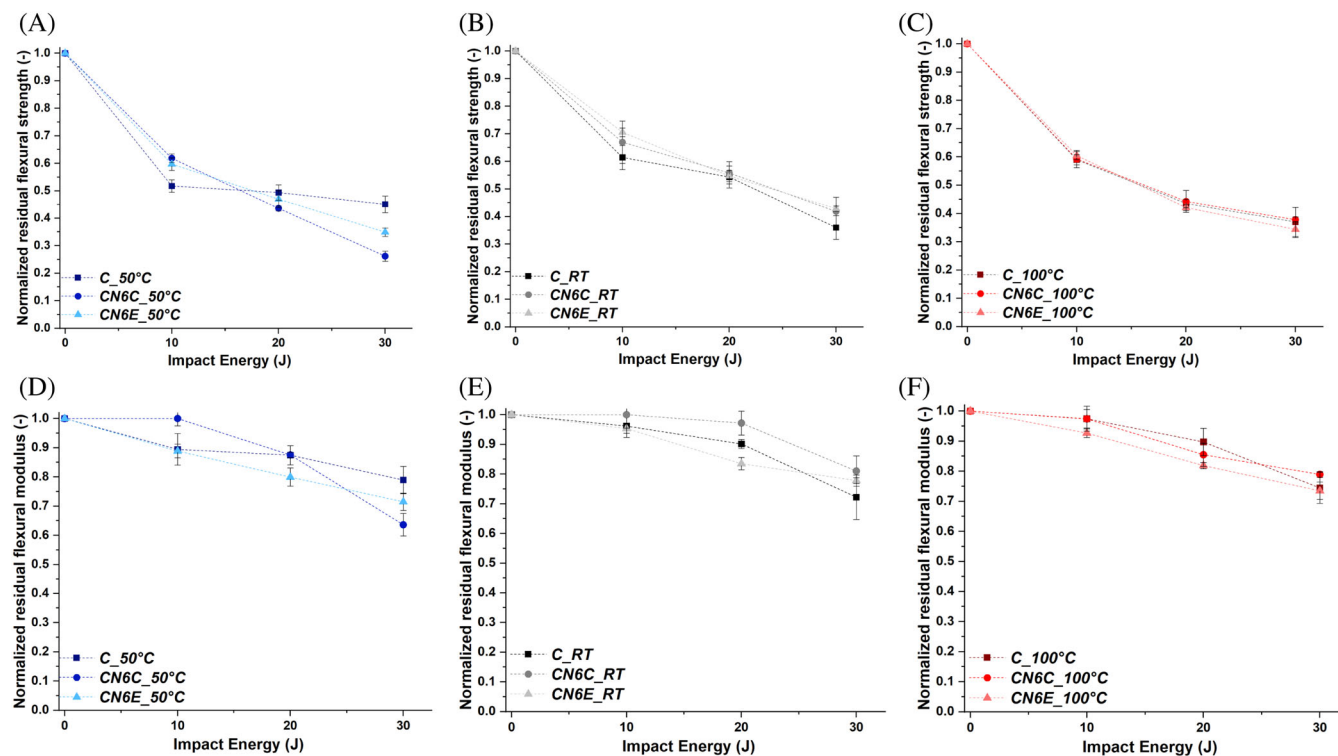


**FIGURE 9** Normalized residual flexural (A, B, C) strength and (D, E, F) modulus after impact of the interleaved laminates compared with the reference C.

CN6E and 9.2% (10 J) and 21.8% (20 J) for CN6C. Only for CN6E, a reduction in delaminated area extent of about 15.7% (10 J) and 12.2% (20 J) was measured. This suggests that in both cases, the veils contribute to additional energy dissipation mechanisms such as nanofiber pull-out and straining, as observed in previous works.<sup>29,49</sup> In Section 3.1, during the LVI tests at room temperature, the outer layers were particularly involved in delamination (Figure 3), and the veils in such a position contributed to minimizing its propagation while the introduction of the veils in the middle plane acted as an additional intra-laminar damage mechanism (green area in Figure 8). At 30 J, the extent of the damage in laminate C is so significant, indicating an extreme failure of the matrix and fibers, that the veils, regardless of their position, lose their effectiveness. Only in CN6E, the delamination extent is limited, showing an increase of about 8.6% compared to 78.9% in CN6C.

These effects are amplified during tests at extreme temperatures ( $-50$  and  $100^{\circ}\text{C}$ ) due to the embrittlement of the veils at low temperatures (glass transition temperature  $\approx 44$ – $60^{\circ}\text{C}$ <sup>50</sup>) and to the overcoming of veils glass transition temperature at high temperature, which is responsible for significant plastic deformation of the nanofibers<sup>27</sup> and contributes to promoting intra-laminar damage in the layers already more susceptible to this damage (Figures 3 and 8). At 10 J, the nanofibers at the outer layers help to direct the energy consumption towards localized deformation, and

delamination, limiting fiber fracture in tension at  $-50^{\circ}\text{C}$ . At  $100^{\circ}\text{C}$ , delamination is slightly reduced compared to C at the same impact condition. At higher impact energy levels, the damage event involves the entire laminate with a significant loss of integrity. However, the reduced extent of fiber fracture at the lowest temperature (Figure S3) and the slight increase in delaminated area (Table 3) provided by the CN6E configuration result in a loss of structural integrity (Figure 7B,D,F), which is, however, lower than CN6C configuration.

The impact event and the resulting damages have a significant effect on the residual mechanical properties of the laminates. In the non-impacted CN6E, the benefits of the veils as a toughening agent are highlighted by the increased bending strength and modulus. This improvement is attributed to the position of veils in the compression-loaded surface where failure begins. In both configurations, the moduli are higher than the C laminate, thanks to the enhancement of carbon fiber-matrix adhesion promoted by the electrospun veils, as illustrated in Figure 10A, where carbon fibers are embedded in the polymer matrix on the interleaved layer. As expected, the impact event has again a detrimental effect on the flexural strength and moduli (Table 4), showing a similar trend as normalized values (Figure 9). Nevertheless, the presence of the veils ensures post-impact flexural properties superior to the reference laminate, demonstrating their effectiveness

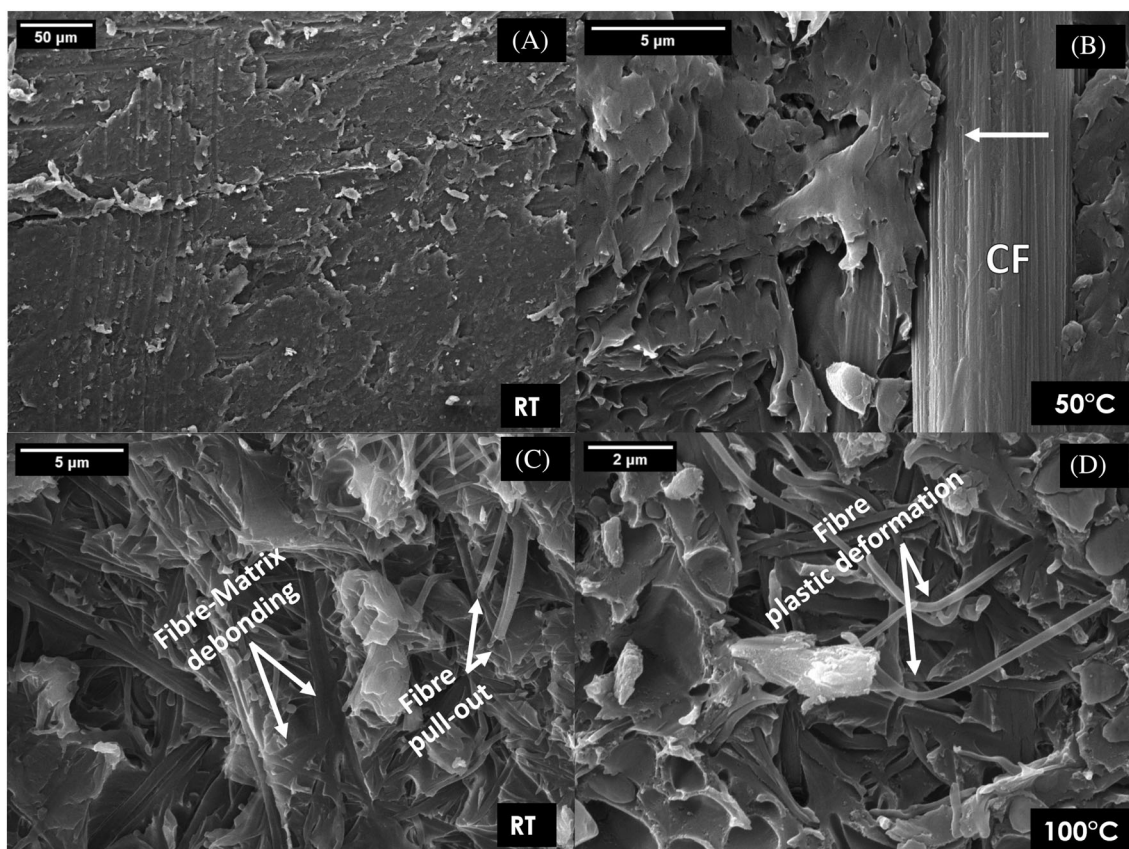


FIGURE 10 Fracture surfaces after flexural tests of interleaved laminates impacted at different temperatures.

in enhancing the damage tolerance of the laminate. Specifically, the flexural strength of interleaved configurations was higher than the C reference, albeit to different extents: by 19.0% (CN6C, at  $-50^{\circ}\text{C}$ ), 26.0% (CN6E, at  $-50^{\circ}\text{C}$ ), and 12.0% (CN6E, at  $100^{\circ}\text{C}$ ) after a 10 J impact; by 4.18% (CN6E, at  $-50^{\circ}\text{C}$ ), 1.29% (CN6C, at  $100^{\circ}\text{C}$ ), and 5.93% (CN6E, at  $100^{\circ}\text{C}$ ) after a 20 J impact; and by 1.78% (CN6C, at  $100^{\circ}\text{C}$ ) and 1.72% (CN6E, at  $100^{\circ}\text{C}$ ) after a 30 J impact. Since the bending tests were conducted at room temperature, it is likely that the electrospun nanofibers, following the previously promoted delamination, are free to act as a bridging network.<sup>28,49,51</sup> This effect is not seen in interleaved laminates when extensive damage, in terms of dent depth and delamination, becomes predominant, resulting in worse damage tolerance compared to the reference C, in particular for CN6E impacted at 30 J and  $-50^{\circ}\text{C}$  and CN6C from an impact energy level of 20 J at  $-50^{\circ}\text{C}$ . At such impact conditions, both laminates showed a flexural strength lower than C due to the occurrence of the highest delaminated area, quantified also in terms of impact energy factor<sup>29</sup> equal to  $9.72\text{ mJ/mm}^2$ , lower than that of C ( $27\text{ mJ/mm}^2$ ). This decrease in damage tolerance was also demonstrated by Jefferson et al. during tensile after impact tests on glass/epoxy laminates, impacted at room temperature with energy levels similar to those used in this study.<sup>52</sup>

Such evidence clearly highlights the suitability of electrospun nanoveils as toughening elements at room and higher temperatures, but makes questionable their exploitation in cryogenic conditions thus making necessary the evaluation of their feasibility according to the final application of the laminate.

SEM micrographs of the fracture surfaces of impacted CN6C and CN6E after bending tests are presented in Figure 10. In general, the presence of the veils contributed to strengthening the interfacial adhesion, preventing interlaminar crack propagation. However, at  $-50^{\circ}\text{C}$ , the embrittlement of the veils is responsible for poor interfacial adhesion between the carbon fiber and the polymer (arrow in Figure 10B), supporting the earlier discussions on the promotion of delamination at the interleaved layers. The pull-out, debonding, and plastic deformation of the nanofibers, proposed as additional energy consuming mechanisms at room temperature,<sup>53</sup> are visible in Figure 10C,D.

#### 4 | CONCLUSION

In conclusion, the analysis of the CFRP performances under extreme temperatures is essential to provide a more complete description of material properties under

different in-service conditions. This study aimed to comprehensively analyze the performance of 2/2 twill CFRP composites interleaved with electrospun thermoplastic veils under low-velocity impact conditions at three impact energy levels (10, 20, and 30 J) and three temperatures ( $-50^{\circ}\text{C}$ , room temperature, and  $100^{\circ}\text{C}$ ). The damage tolerance of CFRP laminates during low-velocity impact events varies significantly with the impact temperature. Different damage modes, including delamination, indentation, and back surface fiber cracking, are observed. Back surface fiber cracking and a through the thickness damage are the typical damage modes at lower temperatures, whereas more pronounced delamination in the upper layers of the laminates characterizes the specimens impacted at higher temperatures.

The influence of veils in laminates varies depending on the impact energy and temperature: in the CN6C configuration, veils did not reduce delaminated area at all energy and temperature conditions tested. However, the CN6E configuration effectively limited delamination extension at room temperature up to an impact energy level of 20 J, thanks to additional energy dissipation mechanisms such as nanofiber pull-out, debonding, and plastic deformation at the layers where delamination prevails. Conversely, the same CN6E configuration proved ineffective in restraining delamination extension for the extreme temperature conditions, except for the impact test at 10 J and  $100^{\circ}\text{C}$  where the further extension of the delaminated area was prevented.

Both interleaved configurations improved the bending properties of the CFRP laminate and enabled good residual post-impact properties at both room temperature and  $100^{\circ}\text{C}$ . However, the substantial damage observed during the impacts at  $-50^{\circ}\text{C}$  led to a significant decrease in normalized residual flexural properties for CN6C (from 20 J) and CN6E (at 30 J). This decrease was attributed to damage concentration on the upper and lower sides of the laminates, which experience higher compressive and tensile loads during bending, respectively.

## DATA AVAILABILITY STATEMENT

Data will be made available on request.

## ORCID

Irene Bavasso  <https://orcid.org/0000-0003-2736-4915>

Claudia Sergi  <https://orcid.org/0000-0002-1232-1560>

## REFERENCES

- Hegde S, Satish Shenoy B, Chethan KN. Review on carbon fiber reinforced polymer (CFRP) and their mechanical performance. *Materials Today: Proceedings*. Vol 19. Elsevier Ltd; 2019:658-662. doi:10.1016/j.matpr.2019.07.749
- Ren Y, Xu L, Sun Y, et al. Study on oxidation behavior during process of recycling carbon fibers from CFRP by pyrolysis. *J Environ Manag*. 2023;347:347. doi:10.1016/j.jenvman.2023.119103
- Körbelin J, Derra M, Fiedler B. Influence of temperature and impact energy on low velocity impact damage severity in CFRP. *Compos Part A Appl Sci Manuf*. 2018;115:76-87. doi:10.1016/j.compositesa.2018.09.010
- Russo A, Zarrelli M, Sellitto A, Riccio A. Fiber bridging induced toughening effects on the delamination behavior of composite stiffened panels under bending loading: a numerical/experimental study. *Materials*. 2019;12(15):1-14. doi:10.3390/ma12152407
- Zhang X, Wu X, He Y, et al. CFRP barely visible impact damage inspection based on an ultrasound wave distortion indicator. *Compos Part B Eng*. 2019;168:152-158. doi:10.1016/j.compositesb.2018.12.092
- Saeedifar M, Najafabadi MA, Zarouchas D, Toudeshky HH, Jalalvand M. Barely visible impact damage assessment in laminated composites using acoustic emission. *Compos Part B Eng*. 2018;152:180-192. doi:10.1016/j.compositesb.2018.07.016
- Wei Q, Zhu L, Zhu J, Zhuo L, Hao W, Xie W. Characterization of impact fatigue damage in CFRP composites using nonlinear acoustic resonance method. *Compos Struct*. 2020;253:253. doi:10.1016/j.compstruct.2020.112804
- Zucchelli A, Focarete ML, Gualandi C, Ramakrishna S. Electrospun nanofibers for enhancing structural performance of composite materials. *Polym Adv Technol*. 2011;22(3):339-349. doi:10.1002/pat.1837
- Sasidharan S, Anand A. Interleaving in composites for high-performance structural applications. *Ind Eng Chem Res*. 2023; 62(1):16-39. doi:10.1021/acs.iecr.2c03061
- Liu Y, Wang G d, Shen Y, Blackie E, He L. Mode-II fracture toughness of carbon fiber reinforced polymer composites interleaved with polyethersulfone (PES)/carbon nanotubes (CNTs). *Compos Struct*. 2023;320:320. doi:10.1016/j.compstruct.2023.117214
- Sihn S, Kim RY, Huh W, Lee KH, Roy AK. Improvement of damage resistance in laminated composites with electrospun nano-interlayers. *Compos Sci Technol*. 2008;68(3-4):673-683. doi:10.1016/j.compscitech.2007.09.015
- Chen Q, Zhang L, Rahman A, Zhou Z, Wu XF, Fong H. Hybrid multi-scale epoxy composite made of conventional carbon fiber fabrics with interlaminar regions containing electrospun carbon nanofiber mats. *Compos Part A Appl Sci Manuf*. 2011; 42(12):2036-2042. doi:10.1016/j.compositesa.2011.09.010
- Chen B, Cai H, Mao C, Gan Y, Wei Y. Toughening and rapid self-healing for carbon fiber/epoxy composites based on electrospinning thermoplastic polyamide nanofiber. *Polym Compos*. 2022;43(5):3124-3135. doi:10.1002/pc.26605
- Brugo T, Minak G, Zucchelli A, et al. Study on mode I fatigue behaviour of nylon 6,6 nanoreinforced CFRP laminates. *Compos Struct*. 2017;164:51-57. doi:10.1016/j.compstruct.2016.12.070
- Akangah P, Lingaiah S, Shivakumar K. Effect of Nylon-66 nano-fiber interleaving on impact damage resistance of epoxy/carbon fiber composite laminates. *Compos Struct*. 2010; 92:1432-1439. doi:10.1016/j.compstruct.2009.11.009
- Hamer S, Leibovich H, Green A, et al. Mode I Interlaminar fracture toughness of nylon 66 Nanofibrilmat interleaved

- carbon/epoxy laminates. *Polym Compos.* 2011;32(11):1689-1903. doi:10.1002/pc
17. Palazzetti R, Zucchelli A, Gualandi C, et al. Influence of electrospun nylon 6,6 nanofibrous mats on the interlaminar properties of gr-epoxy composite laminates. *Compos Struct.* 2012;94(2):571-579. doi:10.1016/j.compstruct.2011.08.019
  18. Alessi S, Filippo MD, Dispenza C, et al. Effects of nylon 6,6 Nanofibrous Mats on thermal properties and delamination behavior of high performance CFRP laminates. *Polym Compos.* 2015;36(7):1303-1313. doi:10.1002/pc.23035
  19. Palazzetti R, Yan X, Zucchelli A. Influence of geometrical features of electrospun nylon 6,6 interleave on the CFRP laminates mechanical properties. *Polym Compos.* 2014;35(1):137-150. doi:10.1002/pc.22643
  20. Mohammadi R, Ahmadi Najafabadi M, Saghafi H, Saeedifar M, Zarouchas D. A quantitative assessment of the damage mechanisms of CFRP laminates interleaved by PA66 electrospun nanofibers using acoustic emission. *Compos Struct.* 2021;258:258. doi:10.1016/j.compstruct.2020.113395
  21. Zheng W, Yao Z, Zhou J, Fan H, Chen W. Microstructure, hygrothermal, and mechanical properties of interlaminar toughening of CFRP composite using polyamide veil. *High Perform Polym.* 2020;32(9):1019-1030. doi:10.1177/0954008320911696
  22. Brugo TM, Minak G, Zucchelli A, Saghafi H, Fotouhi M. An investigation on the fatigue based delamination of woven carbon-epoxy composite laminates reinforced with polyamide nanofibers. *Procedia Eng.* 2015;109:65-72. doi:10.1016/j.proeng.2015.06.208
  23. Beckermann GW, Pickering KL. Mode I and mode II interlaminar fracture toughness of composite laminates interleaved with electrospun nanofibre veils. *Compos Part A Appl Sci Manuf.* 2015;72:11-21. doi:10.1016/J.COMPOSITESA.2015.01.028
  24. Zhang H, Bharti A, Li Z, Du S, Bilotti E, Peijs T. Localized toughening of carbon/epoxy laminates using dissolvable thermoplastic interleaves and electrospun fibres. *Compos Part A Appl Sci Manuf.* 2015;79:116-126. doi:10.1016/j.compositesa.2015.09.024
  25. Daelemans L, van der Heijden S, De Baere I, Rahier H, Van Paeppegem W, De Clerck K. Nanofibre bridging as a toughening mechanism in carbon/epoxy composite laminates interleaved with electrospun polyamide nanofibrous veils. *Compos Sci Technol.* 2015;117:244-256. doi:10.1016/j.compscitech.2015.06.021
  26. Daelemans L, van der Heijden S, De Baere I, Rahier H, Van Paeppegem W, De Clerck K. Using aligned nanofibres for identifying the toughening micromechanisms in nanofibre interleaved laminates. *Compos Sci Technol.* 2016;124:17-26. doi:10.1016/j.compscitech.2015.11.021
  27. Saeedifar M, Saghafi H, Mohammadi R, Zarouchas D. Temperature dependency of the toughening capability of electrospun PA66 nanofibers for carbon/epoxy laminates. *Compos Sci Technol.* 2021;216:216. doi:10.1016/j.compscitech.2021.109061
  28. Palazzetti R, Zucchelli A, Trendafilova I. The self-reinforcing effect of nylon 6,6 nano-fibres on CFRP laminates subjected to low velocity impact. *Compos Struct.* 2013;106:661-671. doi:10.1016/j.compstruct.2013.07.021
  29. Sarasini F, Tirillò J, Bavasso I, et al. Effect of electrospun nanofibres and MWCNTs on the low velocity impact response of carbon fibre laminates. *Compos Struct.* 2020;234:234. doi:10.1016/j.compstruct.2019.111776
  30. Han CL, Wang GD, Li N, Wang M, Liang LX, He MJ. Study on interlaminar performance of CNTs/epoxy film enhanced GFRP under low-temperature cycle. *Compos Struct.* 2021;272:272. doi:10.1016/j.compstruct.2021.114191
  31. Suvarna R, Arumugam V, Bull DJ, Chambers AR, Santulli C. Effect of temperature on low velocity impact damage and post-impact flexural strength of CFRP assessed using ultrasonic C-scan and micro-focus computed tomography. *Compos Part B Eng.* 2014;66:58-64. doi:10.1016/j.compositesb.2014.04.028
  32. Im KH, Cha CS, Kim SK, Yang IY. Effects of temperature on impact damages in CFRP composite laminates. *Compos Part B.* 2001;32:669-682. doi:10.1016/S1359-8368(01)00046-4
  33. Papa I, Langella A, Lopresto V. CFRP laminates under low-velocity impact conditions: influence of matrix and temperature. *Polym Eng Sci.* 2019;59(12):2429-2437. doi:10.1002/pen.25102
  34. Gómez-del Río T, Zaera R, Barbero E, Navarro C. Damage in CFRPs due to low velocity impact at low temperature. *Compos Part B Eng.* 2005;36(1):41-50. doi:10.1016/j.compositesb.2004.04.003
  35. Bhudolia SK, Joshi SC. Low-velocity impact response of carbon fibre composites with novel liquid Methylmethacrylate thermoplastic matrix. *Compos Struct.* 2018;203:696-708. doi:10.1016/j.compstruct.2018.07.066
  36. Ma HL, Jia Z, Lau KT, Leng J, Hui D. Impact properties of glass fiber/epoxy composites at cryogenic environment. *Compos Part B Eng.* 2016;92:210-217. doi:10.1016/j.compositesb.2016.02.013
  37. Salehi-Khojin A, Bashirzadeh R, Mahinfalah M, Nakhaei-Jazar R. The role of temperature on impact properties of Kevlar/fiberglass composite laminates. *Compos Part B Eng.* 2006;37(7-8):593-602. doi:10.1016/j.compositesb.2006.03.009
  38. Katafiasz TJ, Greenhalgh ES, Allegri G, Pinho ST, Robinson P. The influence of temperature and moisture on the mode I fracture toughness and associated fracture morphology of a highly toughened aerospace CFRP. *Compos Part A Appl Sci Manuf.* 2021;142:142. doi:10.1016/j.compositesa.2020.106241
  39. Liu S, Rawat P, Chen Z, Zhu D. Low-velocity impact behavior of carbon woven laminates after exposure to varying temperatures. *Thin-Walled Struct.* 2022;179:179. doi:10.1016/j.tws.2022.109636
  40. Wang Y, Zhang J, Fang G, Zhang J, Zhou Z, Wang S. Influence of temperature on the impact behavior of woven-ply carbon fiber reinforced thermoplastic composites. *Compos Struct.* 2018;185:435-445. doi:10.1016/j.compstruct.2017.11.056
  41. Sánchez-Sáez S, Gómez-Del Río T, Barbero E, Zaera R, Navarro C. Static Behavior of CFRPs at Low Temperatures. [www.elsevier.com/locate/compositesb](http://www.elsevier.com/locate/compositesb)
  42. Fang Y, Fang Z, Jiang R, Jiang Z, Zhu D. Effect of temperature on the transverse impact performance of preloaded CFRP wire. *Compos Struct.* 2020;231:231. doi:10.1016/j.compstruct.2019.111464
  43. Hongkarnjanakul N, Bouvet C, Rivallant S. Validation of low velocity impact modelling on different stacking sequences of CFRP laminates and influence of fibre failure. *Compos Struct.* 2013;106:549-559. doi:10.1016/j.compstruct.2013.07.008
  44. Sergi C, Ierardo N, Lampani L, et al. Low-velocity impact response of MWCNTs toughened CFRP composites: stacking sequence and temperature effects. *Thin-Walled Struct.* 2022;175:175. doi:10.1016/j.tws.2022.109182
  45. Dong K, Peng X, Zhang J, Gu B, Sun B. Temperature-dependent thermal expansion behaviors of carbon fiber/epoxy plain woven composites: experimental and numerical studies. *Compos Struct.* 2017;176:329-341. doi:10.1016/j.compstruct.2017.05.036

46. Rathore DK, Prusty RK, Mohanty SC, Singh BP, Ray BC. In-situ elevated temperature flexural and creep response of inter-ply glass/carbon hybrid FRP composites. *Mech Mater.* 2017;105:99-111. doi:[10.1016/j.mechmat.2016.11.013](https://doi.org/10.1016/j.mechmat.2016.11.013)
47. Icten BM, Atas C, Aktas M, Karakuzu R. Low temperature effect on impact response of quasi-isotropic glass/epoxy laminated plates. *Compos Struct.* 2009;91(3):318-323. doi:[10.1016/j.compstruct.2009.05.010](https://doi.org/10.1016/j.compstruct.2009.05.010)
48. Zhang ZY, Richardson MOW. Low velocity impact induced damage evaluation and its effect on the residual flexural properties of pultruded GRP composites. *Compos Struct.* 2007;81(2): 195-201. doi:[10.1016/j.compstruct.2006.08.019](https://doi.org/10.1016/j.compstruct.2006.08.019)
49. Bavasso I, Tirillò J, Lampani L, Sarasini F. Effect of ZnO-decorated electrospun veils on the damage tolerance of CFRP laminates. *Compos Commun.* 2023;40:40. doi:[10.1016/j.coco.2023.101619](https://doi.org/10.1016/j.coco.2023.101619)
50. Zussman E, Burman M, Yarin AL, Khalfin R, Cohen Y. Tensile deformation of electrospun nylon-6,6 nanofibers. *J Polym Sci B.* 2006;44(10):1482-1489. doi:[10.1002/polb.20803](https://doi.org/10.1002/polb.20803)
51. Marino SG, Košťáková EK, Czél G. Development of pseudo-ductile interlayer hybrid composites of standard thickness plies by interleaving polyamide 6 nanofibrous layers. *Compos Sci Technol.* 2023;234:234. doi:[10.1016/j.compscitech.2023.109924](https://doi.org/10.1016/j.compscitech.2023.109924)
52. Jefferson AJ, Srinivasan SM, Arockiarajan A. Effect of multiphase fiber system and stacking sequence on low-velocity impact and residual tensile behavior of glass/epoxy composite laminates. *Polym Compos.* 2019;40(4):1450-1462. doi:[10.1002/pc.24884](https://doi.org/10.1002/pc.24884)
53. Huang Y, Lv X, Huo H, et al. Interlaminar reinforced carbon fiber/epoxy composites by electrospun ultrafine hybrid fibers. *Compos Part B Eng.* 2024;281:281. doi:[10.1016/j.compositesb.2024.111578](https://doi.org/10.1016/j.compositesb.2024.111578)

## SUPPORTING INFORMATION

Additional supporting information can be found online in the Supporting Information section at the end of this article.

**How to cite this article:** Bavasso I, Sergi C, Ferrante L, et al. Extreme temperature influence on low velocity impact damage and residual flexural properties of CFRP. *Polym Compos.* 2024; 1-16. doi:[10.1002/pc.29029](https://doi.org/10.1002/pc.29029)